A deep learning approach to the inverse problem of modulus identification in elasticity

Bo Ni
School of Engineering, Brown University
Box D, 182 Hope Street, Providence, Rhode Island 02912, United States
bo_ni@brown.edu
ORCID ID: https://orcid.org/0000-0003-2537-591X

Huajian Gao*
School of Mechanical and Aerospace Engineering, College of Engineering, Nanyang Technological University, 70 Nanyang Drive, Singapore 639798, Singapore; Institute of High Performance Computing, A*STAR, Singapore 138632, Singapore
huajian.gao@ntu.edu.sg
ORCID ID: https://orcid.org/0000-0002-8656-846X
* Corresponding author

ABSTRACT

Identifying elastic modulus distribution based on displacement/strain images in elastography and other non-destructive evaluation (NDE) techniques can be challenging, especially when real-time response and high-throughput applications are in demand. In this letter, to address this inverse problem challenge, we propose a deep learning (DL) approach and demonstrate its advantages in achieving high efficiency and accuracy. By carefully designing the sampling spaces of smooth distributions of shear modulus, we demonstrate that a conditional generative adversarial network (cGAN) can successfully learn the high-dimensional mapping between distributions of strain and shear modulus under a compression test, even if trained over a limited portion (20%) of the sample space. At deployment, this model needs not to solve any variational problems proposed in conventional methods and achieves good accuracy (99%). This DL approach has potential for applications in real-time elastography and high-throughput NDE techniques.

IMPACT STATEMENT

Non-destructive evaluation (NDE) of elastic modulus in materials has broad applications in fields such as geological exploration, quality evaluation and medical diagnosis. A key to these techniques is to solve the inverse problem of identifying the distribution of elastic modulus. While conventional theories and numerical methods often involve solving multiple variational problems iteratively for each individual case, the demand of real-time response and high-throughput application of NDE is growing, especially for advanced manufacturing and clinical practices.

To address this challenge, in this letter, we leverage some of the recent progress in data science and propose a deep learning (DL) approach to solve the inverse problem of modulus identification in elasticity. By designing the sampling spaces of smooth distribution of shear modulus and adopting a conditional generative adversarial network (cGAN), we demonstrate that the DL approach can learn the high-dimensional mapping between distributions of strain and shear modulus via training over a limited portion of data. Also, the model can be rapidly deployed with high accuracy, bypassing the iterative solving process in the conventional methods. This work broadens the way of solving challenging inverse problems that aim for applications in real-time elastography and high-throughput NDE techniques.

Keywords: inverse problem, elasticity, deep learning, conditional generative adversarial network, real-time response, high throughput

INTRODUCTION

Due to their non-invasive nature, non-destructive evaluation (NDE) techniques for identifying elastic modulus distribution in materials have attracted increasing attention in various fields, ranging from geological exploration (*1, 2*), construction quality control (*3, 4*), composite material evaluation (*5, 6*), to medical diagnosis (*7, 8*). A common core of these techniques is to solve inverse problems in elasticity. For example, elastography aiming at distinguishing tissues based on a quantitative distribution of elastic modulus has gained broad applications in breast tumor characterization and hepatic fibrosis staging (*9*). During a quasi-static ultrasound elastography (*7*), external compression is applied to the tissue of interest and the deformation fields are estimated using two-dimensional (2D) correlation of ultrasound images (Figure 1a and 1b). To identify the abnormal tissues based on elastic heterogeneity (Figure 1c), an inverse problem of reconstructing the distribution of elastic modulus based on the displacement/strain images needs to be addressed. Thus, solving such inverse problems plays key roles in successful applications of elastography.

Generally speaking, solving inverse problems of elasticity accurately and efficiently can be challenging, especially when real-time response (*10*) and high-throughput applications (*11*) are in demand. Comparing to the forward problem (i.e., to obtain the deformation field under given elastic properties), the inverse problem is more expensive to solve. The problem to find an elastic modulus distribution that minimizes the difference between the predicted and observed deformation fields is often treated as an optimization task under the constraint of elasticity theory in conventional methods such as the equation error approach (*12*) and adjoint-weighted approach (*13, 14*), and solving a nonlinear optimization problem can be costly in practice. For example, in the adjoint-weighted approach (*13*), the inverse problem is solved through an iterative process that involves multiple forward problems within each iteration. Thus, the total computational cost is far beyond that of solving a forward problem. Also, the whole process needs be repeated for different input of displacement images. At the same time, there is growing demand for real-time response and high-throughput applications as elastography and other

NDE techniques continue to advance in multiple clinical applications and advanced manufacturing. For example, tissue elastography in real time shows promising applications in diagnosing breast, prostate, thyroid and pancreatic diseases, even in hope to substitute biopsy (*15*). Ultrasound based NDE techniques have proven potentials in high-throughput screening and fabrication of laser additive manufactured metallic glasses (*11*). These emerging opportunities and demands are calling for more advances in solving the inverse problem of modulus identification in elasticity with high efficiency and accuracy.

Recent progresses in machine learning (ML) provide a new angle to address this challenge. ML, especially deep learning (DL), has proven capable of learning hidden relations between complex patterns from large amount of data (*16*-*20*). For example, in computer vision, deep convolutional neural networks (CNN) can classify millions of images into thousands of classes with high accuracy approaching or even surpassing human performance (*16*). In engineering applications, after proper training over representative data, DL models can learn nonlinear mapping between density-potential and energy density in density functional theory (DFT) (*17*), many-body interatomic potential in molecular dynamics (*18*), constitutive relations in finite element methods (FEM) (*19*) as well as the temporal and spatial behavior history of a dynamics process (*20*).

The advanced learning capability and accessibility to representative data make DL models promising candidates to tackle the inverse problem in elasticity. First, from a data-driven point of view, finding suitable elastic modulus distribution to generate an observed deformation field relies on capturing the hidden mapping between the two fields. The learning and representation capability of DL models make it possible to target such a high-dimensional nonlinear mapping (Figure 1d). For example, conditional generative adversarial networks (cGAN) can handle mapping between images and find applications in image processing tasks such as image reconstruction, segmentation and detection (*21*-*23*). Also, for the training of DL models, affordable accesses exist to collect reliable data in elasticity problems. By solving the forward problem, which is relatively easy to compute, the data of modulus distribution and deformation field can be obtained (Figure 1e). For

example, FEM can be used to calculate the deformation fields for given modulus distribution to sufficient precision (*24*). Based on these advantages, DL models show unique potential in handling the inverse problem of identifying modulus distribution in elasticity in a data-driven way.

It should be noted that DL models have already been applied to improve the performance of medical imaging including elastography. For example, CNN models have been developed as a robust and accurate method to reconstruct the elastography images of strain field from radio frequency data (*25*). It has been demonstrated that CNN classifiers can learn to distinguish malignant tumors from benign ones in breast lesions based on displacement images in elastography (*26*). However, most of these developments deal with end-to-end applications while the middle step of solving the inverse problem of elasticity is often circumvented (*26*).

In the present work, we focus on the inverse problem of identifying modulus distribution in elasticity itself and propose a DL approach to address this fundamental problem in elasticity. By designing representative sampling spaces for smooth distribution of shear modulus (Figure 1f) and constructing a cGAN model (Figure 1d), we demonstrated that the proposed DL approach can learn the high-dimensional mapping between distributions of strain and shear modulus via training over a limited portion of data and achieve high efficiency and accuracy at deployment.

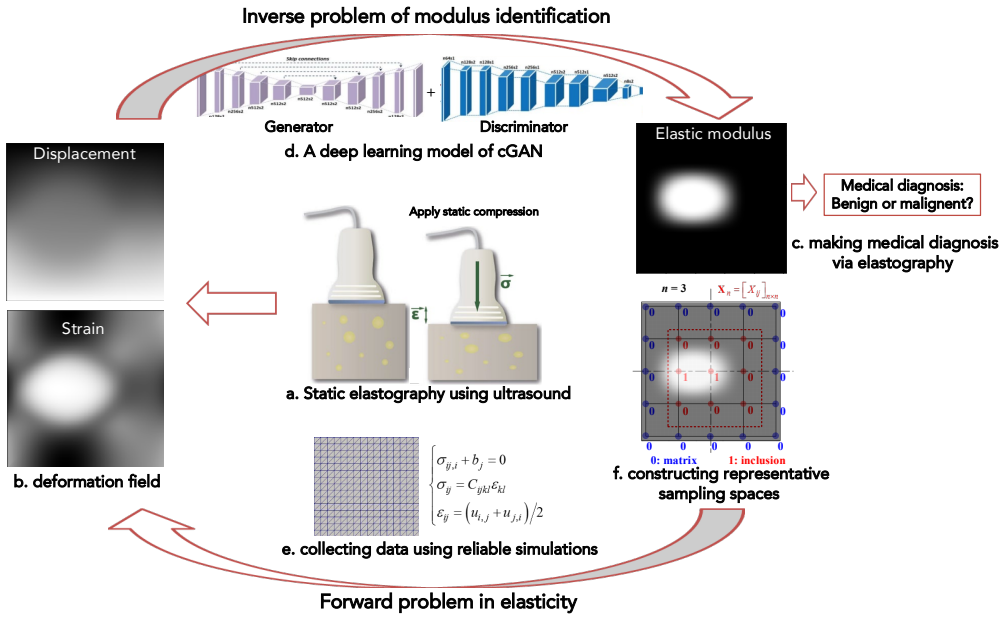

Figure 1. A deep learning approach to the inverse problem of modulus identification in elasticity. (a) A schematic of static elastography using ultrasound. (b) Simulated images of deformation filed obtained from elastography. (c) Making medical diagnosis based on the distribution of elastic modulus. (d) A deep learning model with the structure of cGAN. (e) Collecting data by solving the forward problem of elasticity with reliable numerical simulations. (f) Constructing representative sampling spaces for the distribution of elastic modulus.

RESULTS

Without loss of the generality, the present work borrows the set-up of a static elastography using ultrasound and focuses on a prototype inverse problem of identifying the distribution of shear modulus of a nearly incompressible elastic material based on strain images (*13*). As shown in Figure 2a, a nearly incompressible isotropic linear elastic material occupies a 2D domain, $\Omega = (0, L) \times (0, L)$. A uniaxial compressive load is applied along the vertical direction by prescribing the displacement on the top and bottom edges with $u_2 = 0 @ x_2 = 0$ and $u_2 = -0.001L @ x_2 = L$ while the left and right remain traction-free. To avoid rigid body translation, the origin is fixed horizontally with $u_1 = 0 @ (0,0)$. The distribution of the strain component, $\varepsilon_{22}(x_1, x_2)$, also called elastogram, is obtained by processing ultrasound measurements. The inverse problem is to recover the distribution of shear modulus, $\mu(x_1, x_2)$, based on the strain image of ε_{22}. To avoid

the ill-posedness of the inverse problem, we assume the shear modulus to be constant on the edges (*27*).

The goal here is to present a DL approach to address a prototype inverse problem in elasticity. We demonstrate that, by collecting reliable data over representative sampling spaces and capturing the mapping between strain and modulus with a suitable cGAN model, the DL approach can achieve high efficiency and accuracy at deployment. The DL approach developed here can be easily extended for other specific cases and applications.

Building representative sampling spaces

In the DL approach, the underlying relation between shear modulus and strain filed is conveyed implicitly via data. Thus, collecting relevant and representative data often plays a key role in such a data-driven approach.

While the possible distributions of shear modulus can be infinite, here we mimic the situation in breast cancer diagnosis and focus on the relevant matrix-inclusion cases with smooth transition, i.e.,

$$\mu(x_1, x_2) = \mu_M + (\mu_I - \mu_M) \cdot g(x_1, x_2) \tag{1}$$

where μ_M, μ_I are the shear moduli of the matrix and the inclusion, representing healthy glandular tissue and malignant lesion respectively, $g(x_1, x_2) \in [0,1]$ is a normalized function describing the spatial distribution of the two and the smooth transition in-between. Here, we take $\mu_I = 5\mu_M$, which is a typical case for ductal carcinoma *in situ* surrounded by glandular tissue in human breast under small deformation (*28*).

Focusing on the normalized distribution function (NDF) $g(x_1, x_2)$, we construct relevant sampling spaces to approximate some representative cases of the matrix-inclusion geometry. The key features considered include the size, shape and position of the inclusions. To do so, we divide the internal region of domain Ω into a (n+1)-by-(n+1) evenly spaced grid and assign inclusion ($g = 1$) or matrix ($g = 0$) to the (n+2)-by-(n+2) grid points (Figure 2b). To avoid the ill-posedness of the inverse problem, we assume the boundary is occupied by matrix material and choose g = 0 for grid points on the boundary (blue points). The values of the internal

grid points (red ones), X_{ij}, can be 0 or 1, forming a grid matrix, $\mathbf{X}_n = \left[X_{ij} \right]_{n\times n}$. Then, we adopt a cubic spline method to interpolate the gird point values to construct a smooth function $g^h(x_1, x_2; \mathbf{X}_n)$, over the domain Ω, (Figure 2c) satisfying

$$g^h(x_1, x_2; \mathbf{X}_n) \in [0,1] \; and \; g^h = 0 \; @ \; Edges \, . \tag{2}$$

Noting that g^h is uniquely determined by $\mathbf{X}_n$ and there are $2^{n\times n}$ choices for $\mathbf{X}_n$ or g^h, we denote the space of $g^h(x_1, x_2; \mathbf{X}_n)$ as the function sampling space (FSS), $\mathbb{A}_n$, i.e.,

$$\mathbb{A}_n = \left\{ g^h(x_1, x_2; \mathbf{X}_n) : \mathbf{X}_n = \left[X_{ij} \right]_{n\times n}, \, X_{ij} = 0 \; or \; 1, \;\; i, j = 1, 2, ..n \right\} \tag{3}$$

and it is a finite function space with a dimension as the following,

$$\dim\left[\mathbb{A}_n \right] = 2^{n\times n} \, . \tag{4}$$

We can use a series of such FSSs, $\{\mathbb{A}_n\}, n = 2, 3, 4, ...$, to approximate $g(x_1, x_2)$ for the matrix-inclusion cases. Taking n = 4 as an example, for samples belonging to $\mathbb{A}_4$, the number, shape, size and topology of inclusions can vary, representing various matrix-inclusion geometries (see Figure 2d for representative examples and Movie I for more cases). As n increases, the spacing of the grid, $L/(n+1)$, decreases, so does the minimal dimension of the inclusions represented in $\mathbb{A}_n$ (Figure 2e). Correspondingly, the dimension of $\mathbb{A}_n$ increases (Equation (4)) and more complex matrix-inclusion cases can be captured. Here, we focus only on the cases with a finite n, since the region of interest (i.e., domain Ω) in elastography is often finite and only inclusions with a detectable size are of concern.

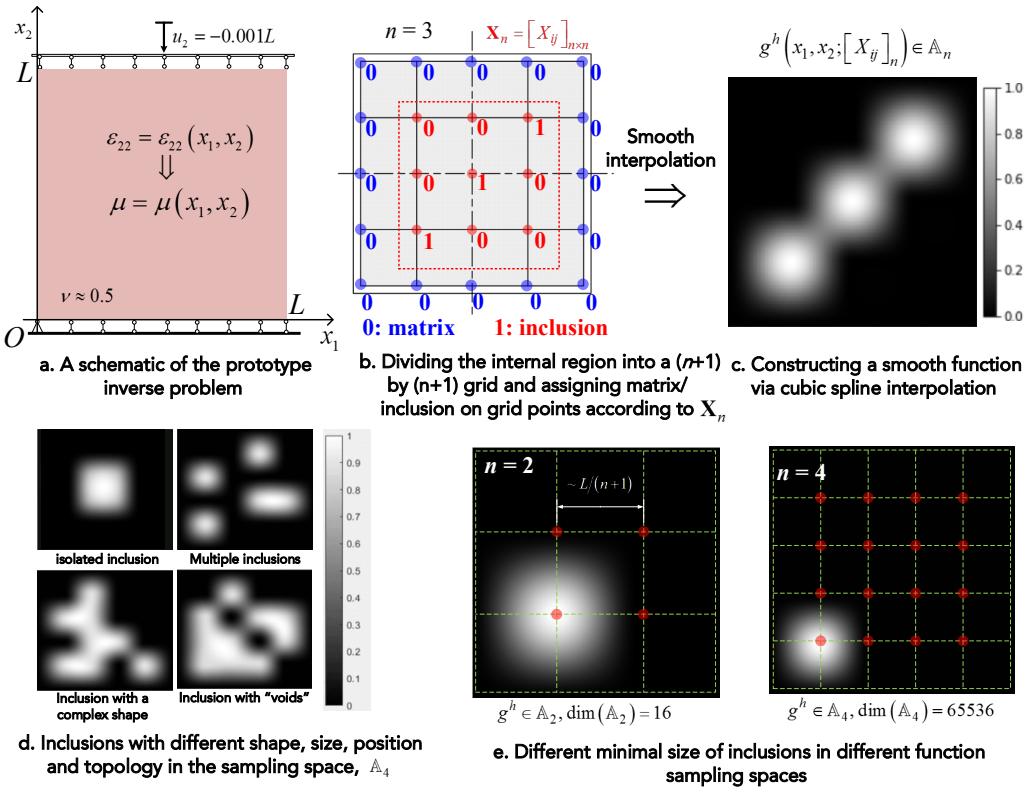

Figure 2. Construction of representative sampling spaces of the relevant matrix-inclusions cases for the prototype inverse problem in elastography. (a) A schematic of the prototype inverse problem. (b) Discretizing the domain with a finite grid and a grid matrix X_n. (c) Constructing a full field distribution of shear modulus based on X_n using spline interpolation. (d) Representative examples with inclusions of different shape, size, position and topology in the sampling space, $\mathbb{A}_4$. (e) Different minimal sizes of inclusions in function sampling spaces of different *n*.

To collect reliable deformation response of samples in $\mathbb{A}_n$ under the test load (Figure 2a), we adopt FEM to solve the forward elasticity problem. Only the strain component along the loading direction, ε_{22}, is collected to mimic the situation in elastography. Write the strain filed as,

$$\varepsilon_{22}(x_1, x_2) = \varepsilon_{\min} + (\varepsilon_{\max} - \varepsilon_{\min}) \cdot f(x_1, x_2) \tag{5}$$

where $\varepsilon_{\min}$, $\varepsilon_{\max}$ are the minimal and maximal strain and $f(x_1, x_2) \in [0,1]$ represents the normalized distribution pattern of the strain. The goal of solving the inverse problem of elasticity in elastography is to figure out $g(x_1, x_2)$ given the measure of $f(x_1, x_2)$. Next, we construct a cGAN model to learn the underlying relation between these two over the constructed sampling space.

A cGAN model and its performance

We leverage the recent development of image-to-image translation in ML study and construct a cGAN model to learn the mapping between images of strain and shear modulus. As shown in Figure 3a, $g(x_1, x_2)$ and $f(x_1, x_2)$ are represented by images with 256-by-256 pixels. The cGAN model consists of a U-Net architectured generator and a convolutional "PatchGAN" classifier, which have proven useful in various image-to-image tasks (*22, 23*). Here, the generator aims at creating suitable modulus images conditioned by the input of strain images while the discriminator learns to identify the "fake" modulus images created by the generator from the real ones. Through training, the performance of the two improves adversarially until reaching a Nash equilibrium (*29*), i.e., the generator creates modulus images so real that the trained discriminator cannot distinguish them from the real ones. Beside this adversarial objective, minimizing L_2 loss of the prediction is also mixed in the training objective for better performance, as suggested in previous studies (*30*). Details about the implementation of the cGAN model can be found in the method section.

The performance of the cGAN model is tested over the cases in $\mathbb{A}_4$. Considering the reflection symmetry with respect to the loading, we identify about 16576 unique samples in $\mathbb{A}_4$ and split them into sets of training (70% of the samples), validating (15%) and testing (15%). After trained over the training set for 400 epochs, the cGAN model can make accurate predictions in the testing set, which it has never seen before. For example, three randomly picked examples are shown in Figure 3b and the predicted distributions agree well with the ground truth (More examples can be found in Movie II). On average, a normalized L_2 error, $\bar{E}_{L2}$, of 0.30% is achieved in the testing set (Figure 3c). Beside the accuracy, the well trained cGAN model is also efficient at deployment, as only the generator in the cGAN model is activated when applied to the testing set. Making prediction for one input takes about 0.06 second in a freely accessed Google Codelabs platform. The iterative steps of solving multiple variational problems in the conventional methods for the inverse problem in elasticity, which can take minutes (*13*), is

bypassed for all testing cases in the sampling space. This time-efficiency at deployment makes it promising for applications requiring real-time response.

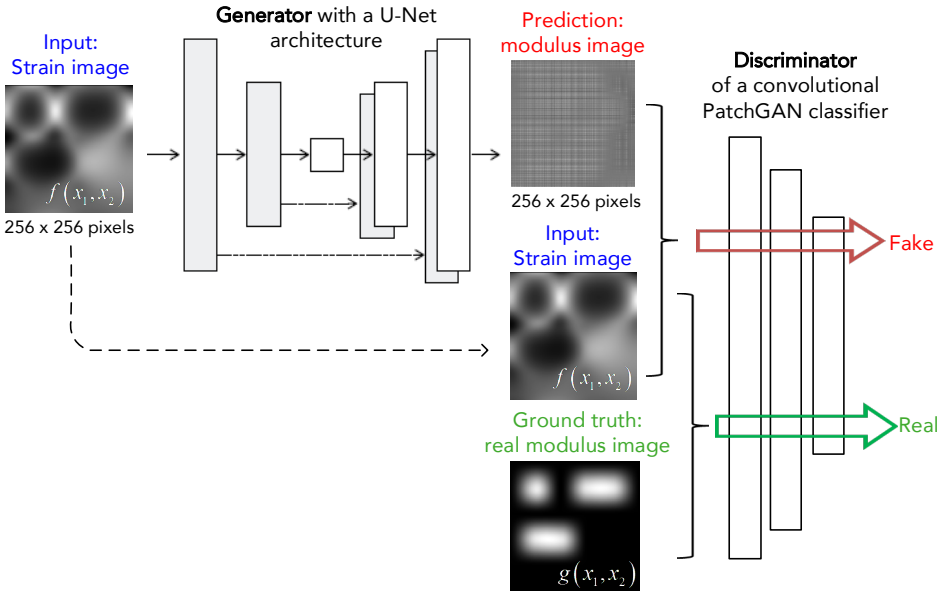

a. A schematic of the cGAN model for strain-modulus mapping

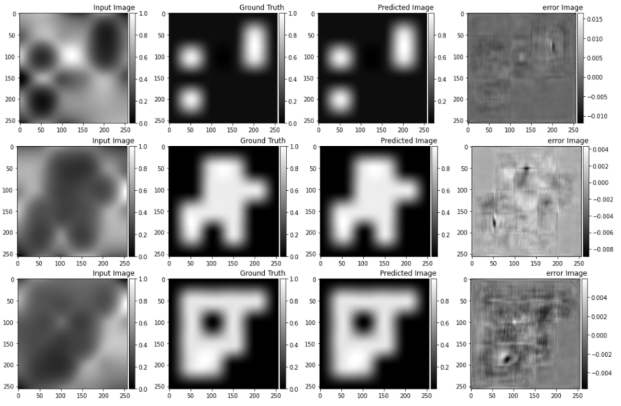

b. Examples of the cGAN model's prediction on the testing set of $\mathbb{A}_4$ after 400 epochs of training

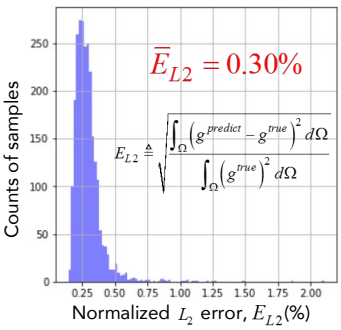

c. Histogram of normalized L_2 error of the cGAN model's prediction on the testing set of $\mathbb{A}_4$ after 400 epochs of training

Figure 3. A cGAN model for the prototype inverse problem in elastography and its predictions on the sampling set $\mathbb{A}_4$. (a) Schematic structure of the cGAN model. (b) Randomly picked examples of the cGAN model's prediction on the testing set in $\mathbb{A}_4$ after 400 epochs of training. (c) The distribution of the normalized L_2 error of the prediction of the cGAN model on the test set after 400 epochs of training.

As a data-driven approach, the DL model learns to solve all cases in the sampling space together through training over a limited portion of the data. To demonstrate this generalized predicting capability, we study the effect of the

training set size on the performance of the cGAN model over the designed FSS. We define the relative sizes of the sets of training, validation and testing as

$$\alpha_{tra} = \frac{N_{tra}}{N_{tot}}, \alpha_{val} = \frac{N_{val}}{N_{tot}}, \alpha_{test} = \frac{N_{test}}{N_{tot}} \quad (6)$$

where N_{tra}, N_{val} and N_{test} are the sizes of the three sets, respectively, N_{tot} is the total number of the unique samples in $\mathbb{A}_4$, and $\alpha_{tra} + \alpha_{val} + \alpha_{test} = 1$. Keeping the relative size of the validation set α_{val} as a constant of 10%, we train six cGAN models from scratch over the training set with the relative size α_{tra} varying from 60% to 10%. As shown in Figure 4a, during the first 200 epochs, the performances of the all the models improves rapidly toward the converged plateau on both the training and testing sets. No overfitting is observed. A close look at the normalized L_2 error curves reveals that larger training set can promote the learning speed (See the zoom-in panel in Figure 4a). After 200 epochs of training, the normalized L_2 errors for the six models are all less than 2% (Figure 4b).

For meaningful applications in elastography tests, here we set an accuracy higher than 99% in the L_2 sense (the black dash line in Figure 4b) as the goal. Benefited from the representativeness of the designed sampling space and the learning capability of the cGAN model, we find training over a 20% portion of the samples for 200 epochs is enough to fulfill this goal and make predictions with a L_2 error less than 1% for the remaining 80% samples in $\mathbb{A}_4$, which the cGAN model has never seen before. This effectiveness of a finite size of the training set further reduces the training cost of the DL model for a targeted accuracy and demonstrate the efficiency of the DL approach in learning the underlying mapping between strain and shear modulus in the designed sampling space. This learning efficiency may open doors to high-throughput applications in NDEs.

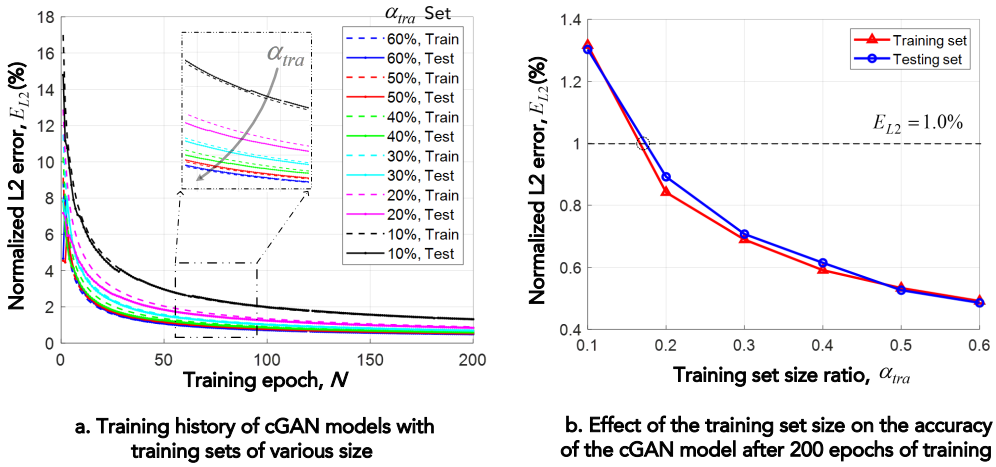

a. Training history of cGAN models with training sets of various size

b. Effect of the training set size on the accuracy of the cGAN model after 200 epochs of training

Figure 4. The effect of training set size on the performance of the cGAN model. (a) Training history of the cGAN models trained over training sets of various size. (d) The performance of cGAN models after trained over training sets of various size for 200 epochs.

DISCUSSION AND CONCLUSION

In this letter, we leverage some of the recent progresses in ML to address the inverse problem of modulus identification in elasticity that involves matrix-inclusion systems mimicking an elastography set-up. By designing representative sampling spaces and constructing capable cGAN models, we demonstrated that the DL approach can efficiently learn the high-dimensional mapping between distributions of strain and shear modulus via training over a limited portion of the samples in the relevant sampling space. At deployment, this approach can response rapidly with high accuracy, bypassing the iterative steps of solving multiple variational problems in the conventional methods. The DL approach broadens the way of addressing challenging inverse problems in real-time elastography and high-throughput NDE applications. Future studies can further build on this and explore the capability of DL-based approaches in handling challenges such as noised data, nonlinearity and ill-posedness for various inverse problems (*31*) in fundamental sciences as well as engineering applications.

MATERIALS AND METHODS

FEM simulations

We perform FEM to solve the boundary value problem in Figure 2a with a mesh of triangular C0 elements with 256x256 evenly distributed nodes. A Poisson

ratio of 0.499 is used to mimic tissues in elastography and the "B-bar" method is adopted to handle this near incompressibility in FEM (*24*). The images of strain and modulus are constructed using the nodal values.

cGAN model

The cGAN model is implemented in Python using TensorFlow (*32*). Both generator and discriminator use the building block in the form of convolution-BatchNorm-ReLu. Detailed structures can be found in the reference (*23*). The cGAN model are trained with the Adam optimizer (*33*) with a learning rate of 0.0002 and momentum parameters $\beta_1 = 0.5, \beta_2 = 0.999$.

ACKNOWLEDGMENTS AND DELARATION OF CONFICTS AND OTHER DISCLOSURES

The authors acknowledge the support by the National Science Foundation (NSF) under the grant CMMI-1634492. The simulations were performed on resources provided by the Extreme Science and Engineering Discovery Environment (XSEDE) through grant MSS090046 and at the Center for Computation and Visualization (CCV) at Brown University.

SUPPLEMENTARY INFORMATION

Movie I: The unique samples in the sampling space $\mathbb{A}_4$ representing various matrix-inclusion geometry.

Movie II: The performance of the DL model on the testing set (15%) after 400-epoch training.

Both movies can be download using the following link.

https://www.dropbox.com/sh/gm1q43vvl20xvrx/AABLh2ZntDZtZdUtZYVq6PLNa?dl=0

REFERENCES

1. M. Rodríguez-Sastre, L. Calleja, The determination of elastic modulus of slates from ultrasonic velocity measurements. *The Geological Society of London. IAEG* **775**, 1-11 (2006).
2. E. Martinho, A. Dionísio, Main geophysical techniques used for non-destructive evaluation in cultural built heritage: a review. *Journal of Geophysics and Engineering* **11**, 053001 (2014).
3. E. Reufi, I. Thomas, Evaluation of modulus of elasticity by non-destructive method of hybrid fiber reinforced concrete. *Int. J. Adv. Chem. Eng. Biol. Sci.* **3**, 1-4 (2016).
4. P. Icenogle, S. Kabir, "Evaluation of non-destructive technologies for construction quality control of HMA and PCC pavements in Louisiana," (Louisiana. Dept. of Transportation and Development, 2013).
5. M. Jalili, A. Pirayeshfar, S. Mousavi, in *29th Eur Conf Aco Emi Test (EWGAE), Vienna, Austria*. (2010).
6. S. Gholizadeh, A review of non-destructive testing methods of composite materials. *Procedia Structural Integrity* **1**, 50-57 (2016).
7. J.-L. Gennisson, T. Deffieux, M. Fink, M. Tanter, Ultrasound elastography: principles and techniques. *Diagnostic and interventional imaging* **94**, 487-495 (2013).
8. J. Bercoff *et al.*, In vivo breast tumor detection using transient elastography. *Ultrasound in medicine & biology* **29**, 1387-1396 (2003).
9. R. M. Sigrist, J. Liau, A. El Kaffas, M. C. Chammas, J. K. Willmann, Ultrasound elastography: review of techniques and clinical applications. *Theranostics* **7**, 1303 (2017).
10. H. Hong *et al.*, Performance of real-time elastography for the staging of hepatic fibrosis: a meta-analysis. *PloS one* **9**, (2014).
11. L. Zhai, Y. Lu, X. Zhao, L. Wang, X. Lu, High-throughput screening of laser additive manufactured metallic glass via ultrasonic wave. *Scientific reports* **9**, 1-6 (2019).
12. E. Crossen, M. S. Gockenbach, B. Jadamba, A. A. Khan, B. Winkler, An equation error approach for the elasticity imaging inverse problem for predicting tumor location. *Computers & Mathematics with Applications* **67**, 122-135 (2014).
13. A. A. Oberai, N. H. Gokhale, G. R. Feijóo, Solution of inverse problems in elasticity imaging using the adjoint method. *Inverse problems* **19**, 297 (2003).
14. N. H. Gokhale, P. E. Barbone, A. A. Oberai, Solution of the nonlinear elasticity imaging inverse problem: the compressible case. *Inverse Problems* **24**, 045010 (2008).
15. L. Feril, Can Ultrasound Elastography Substitute Tissue Biopsy in the Diagnosis of Malignancy. *MJ Cancer* **1**, 004 (2016).
16. A. Krizhevsky, I. Sutskever, G. E. Hinton, in *Advances in neural information processing systems*. (2012), pp. 1097-1105.

17. F. Brockherde *et al.*, Bypassing the Kohn-Sham equations with machine learning. *Nature communications* **8**, 1-10 (2017).
18. H. Wang, L. Zhang, J. Han, E. Weinan, DeePMD-kit: A deep learning package for many-body potential energy representation and molecular dynamics. *Computer Physics Communications* **228**, 178-184 (2018).
19. D. Z. Huang, K. Xu, C. Farhat, E. Darve, Learning constitutive relations from indirect observations using deep neural networks. *Journal of Computational Physics*, 109491 (2020).
20. Y.-C. Hsu, C.-H. Yu, M. J. Buehler, Using Deep Learning to Predict Fracture Patterns in Crystalline Solids. *Matter*, (2020).
21. X. Yi, E. Walia, P. Babyn, Generative adversarial network in medical imaging: A review. *Medical image analysis*, 101552 (2019).
22. M. Mirza, S. Osindero, Conditional generative adversarial nets. *arXiv preprint arXiv:1411.1784*, (2014).
23. P. Isola, J.-Y. Zhu, T. Zhou, A. A. Efros, in *Proceedings of the IEEE conference on computer vision and pattern recognition*. (2017), pp. 1125-1134.
24. A. F. Bower, *Applied mechanics of solids*. (CRC press, 2009).
25. S. Wu *et al.*, in *International Conference on Medical Image Computing and Computer-Assisted Intervention*. (Springer, 2018), pp. 374-382.
26. D. Patel *et al.*, Circumventing the solution of inverse problems in mechanics through deep learning: Application to elasticity imaging. *Computer Methods in Applied Mechanics and Engineering* **353**, 448-466 (2019).
27. P. E. Barbone, J. C. Bamber, Quantitative elasticity imaging: what can and cannot be inferred from strain images. *Physics in Medicine & Biology* **47**, 2147 (2002).
28. P. Wellman, R. D. Howe, E. Dalton, K. A. Kern, Breast tissue stiffness in compression is correlated to histological diagnosis. *Harvard BioRobotics Laboratory Technical Report*, 1-15 (1999).
29. F. Farnia, A. Ozdaglar, GANs May Have No Nash Equilibria. *arXiv preprint arXiv:2002.09124*, (2020).
30. D. Pathak, P. Krahenbuhl, J. Donahue, T. Darrell, A. A. Efros, in *Proceedings of the IEEE conference on computer vision and pattern recognition*. (2016), pp. 2536-2544.
31. M. Bonnet, A. Constantinescu, Inverse problems in elasticity. *Inverse problems* **21**, R1 (2005).
32. M. Abadi *et al.*, in *12th {USENIX} Symposium on Operating Systems Design and Implementation ({OSDI} 16)*. (2016), pp. 265-283.
33. D. P. Kingma, J. Ba, Adam: A method for stochastic optimization. *arXiv preprint arXiv:1412.6980*, (2014).